Journal of Power Sources 255 (2014) 187–196

Contents lists available at ScienceDirect

Journal of Power Sources

journal homepage: www.elsevier.com/locate/jpowsour

A novel air electrode design: A key to high rate capability and long life span

Lun Xu [a,1], Jun Ma [b,c,*,1], Baohua Li [c,*], Feiyu Kang [a,c]

[a] School of Materials Science and Engineering, Tsinghua University, Beijing 100084, China
[b] College of Materials Science and Engineering, Shenzhen University, Shenzhen 518060, China
[c] Advanced Materials Institute, Graduate School at Shenzhen, Tsinghua University, Shenzhen 518055, China

HIGHLIGHTS

- A novel TBGL was designed on the basis of the nature of electrolyte.
- The oxygen concentration along the thickness of the air electrode was calculated.
- Electrochemical reaction mechanisms for the DMSO-based electrolyte were investigated.
- We demonstrated a long-life Li-O_2 battery with high power and energy densities.
- A brand new view was opened up to greatly boost the electrochemical performance.

GRAPHICAL ABSTRACT

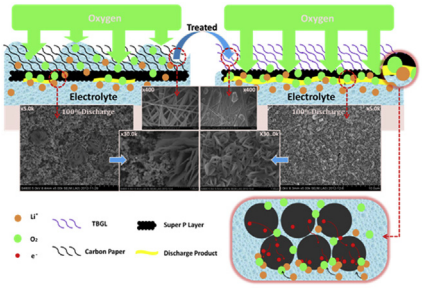

ARTICLE INFO

Article history:
Received 26 October 2013
Received in revised form
20 December 2013
Accepted 29 December 2013
Available online 8 January 2014

Keywords:
Lithium-oxygen batteries
Air electrode
DMSO
Rate capability
Oxygen concentration
Mechanism

ABSTRACT

As an appealing storage system for electric vehicle application, the lithium-oxygen battery could theoretically provide ultrahigh energy density; however, its attractive implementation is overshadowed by unsatisfactory electrochemical characteristics of the poor rate capability and the short span life. Here, we put forward one kind of effective strategy to ameliorate these deficiencies. By embedding a novel air electrode, the utilization level of the electrochemically available active sites is effectively increased and meanwhile the mass transfer of oxygen is signally improved. The evaporation speed of the solvent is greatly slowed down to some degree. We demonstrate that a super P-based lithium-O_2 battery could be operated over stable 50 cycles at the current density of 3000 mA g^{-1}_{Carbon} (equivalent to 2.4 mA cm^{-2}), corresponding to a discharge time of about 20 min to 1000 mAh g^{-1}_{Carbon}. Based on the weight of the super P and the resultant Li_2O_2, the specific power density could reach 4040 W kg^{-1}; even so, a substantial specific energy density of 1350 Wh kg^{-1} still could be achieved.

1. Introduction

In the past decades, the vast majority of the research work has been performed to upgrade the energy and power densities of the conventional lithium-ion battery; however, it is still far less able to satisfy the increasing stringent demands for electrification transportation and super energy storage system. Based upon the overwhelming storage superiority, a rechargeable lithium-oxygen

* Corresponding authors. College of Materials Science and Engineering, Shenzhen University, Shenzhen 518060, China.
E-mail addresses: majun@szu.edu.cn, boykewich@live.cn (J. Ma), libh@mail.sz.tsinghua.edu.cn (B. Li).
[1] These authors contributed equally to this work.

0378-7753/$ – see front matter © 2014 Elsevier B.V. All rights reserved.
http://dx.doi.org/10.1016/j.jpowsour.2013.12.124

battery has stirred a revived interest and attention [1–5]. But so far now, the discharge specific capacity and the cycling stability achieved come in well short of expectation. In the face of its practical applications in the future, there are formidable challenges to be overcome, for example, the reactivity of aprotic electrolyte towards superoxide anion free radical ($O_2^{\cdot-}$) or oxygen [6,7], the poor rate capability, the short calendar life [1,8–10] and the low round-trip efficiency. Most recently, strategies targeted to develop a truly rechargeable Li-O_2 battery with outstanding rate capability and long cycle life have mainly been focused on exploration of the electrolyte formula, design of the air electrode and optimization of the operating parameters [1,2,11–15].

Pioneer work has suggested that the reversibility of the lithium-oxygen battery and the nature of the reduction deposits largely depend on the electrolyte formula, especially the composition of solvent [16]. The electrochemical performances are chiefly determined by the oxygen solubility in electrolyte and the oxygen diffusion velocity through the whole air electrode, especially at high current densities [15]. It is clear that for the high-performance, rechargeable lithium-oxygen batteries, screening for solvent is quite demanding. Consequently, the exploitation of the solvent available for the truly rechargeable nonaqueous Li-O_2 battery is always an elusive puzzle. The powerful nucleophilicity of superoxide ($O_2^{\cdot-}$), which is a primary intermediate in the Li-O_2 battery, or/and the superoxide-mediated oxidation of the hydroperoxides derived in the aprotic solvent are regarded as the first thing to be addressed [6,7,11,12]. Organic carbonates and esters could be easily decomposed at *O*-alkyl or carbonyl carbon via a nucleophilic attack from the superoxide anion radical ($O_2^{\cdot-}$). Most of ether- and amide-based electrolytes, which were once believed to be the stable candidates, were prone to autoxidation under oxygen atmosphere. Furthermore, ethers did not support the reversible formation/decomposition of the desired Li_2O_2 and their stabilities were gradually deteriorated upon cycling [11,16]. This or that deficiency has severely undermined the boost of the electrochemical performance of Li-O_2 battery. Recently, an alcahest dimethyl sulfoxide (DMSO) was much concerned and considered as a promising solvent for Li-O_2 cell, owing to its satisfactory stability against the superoxide radical [17]. However, the relatively lower oxygen solubility and the comparatively higher viscosity are at a disadvantage from the perspective of the electrochemical kinetics. Therefore, it becomes more meaningful to take effective measures to make up its deficiencies.

As another crucial component, a typical porous air electrode mainly consists of a collector (metal grid, metal foam, carbon paper and etc.) and a porous electrode material layer with or without catalyst, as illustrated in Fig. 1. As a vital arena, where Li-O_2 heterogeneous reactions happen and the discharge products are hosted, the porosity and tortuosity of the air electrode will have a significant impact on the electrochemical characteristics of Li-O_2 batteries [2,3,18,19]. Thus, the choice and microstructure design of the air electrode materials come into a paramount important issue. Until now, various carbonaceous materials [8,18–23] (for example, super P, carbon nanofiber, graphene, ketjen black), conductive polymer (polypyrrole [24]) and precious metal (Au [8]) have been investigated as electrode materials aiming to realize the higher discharge capacity and rate capability. In some cases, the transition metal oxide and metal (or alloy) catalysts [16,23,25–31] (Pt, Au, MnO_2 and $MnCo_2O_4$) were exploited to improve the electrochemical properties. The round-trip hysteresis was greatly reduced, however the undesired decompositions/side reactions were often promoted simultaneously [32,33]. Admittedly, the performance level of Li-O_2 cell has gotten a great promotion via quantitatively increasing the solid–liquid interfaces and the storage volumes, provided by the vesicular structure of the air electrode materials themselves or/and the air electrode itself [19]. Unfortunately, these underlying active sites seems not be fully utilized because of the inaccessibility of oxygen.

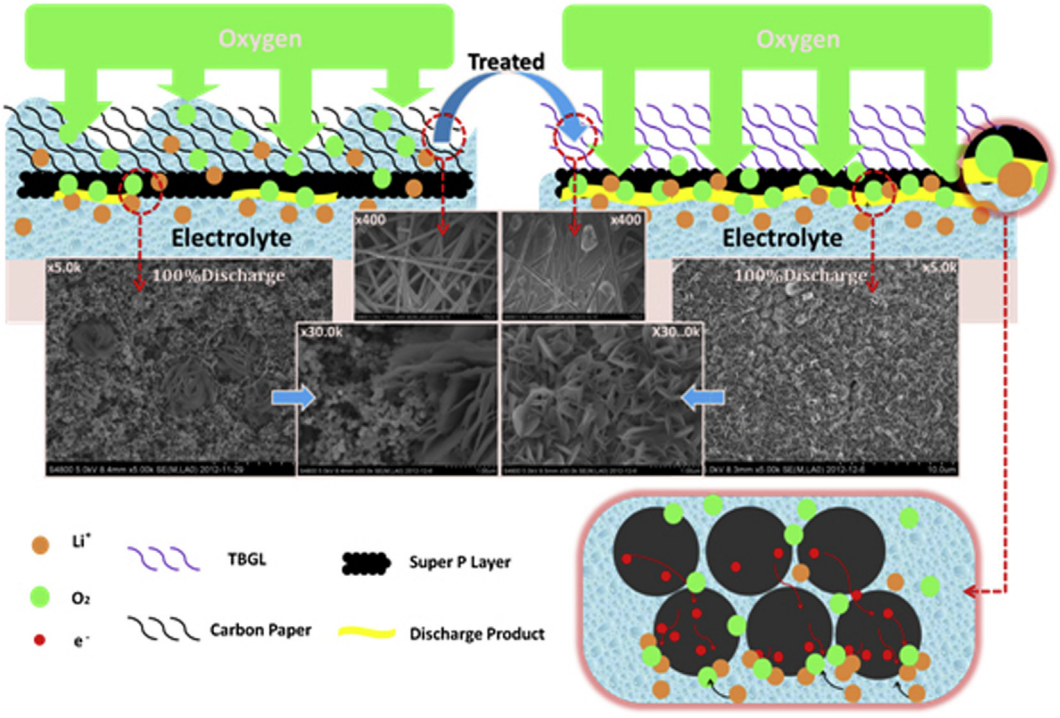

Fig. 1. Schematic diagram of the air electrode configuration. The conventional flooded air electrode on the left and our novel one on the right. Inset: FESEM images for carbon paper and TBGL; and surface morphologies for these two kinds of air electrodes after full discharge.

In almost all the lithium-oxygen electrochemical device, the whole porous electrode was practically flooded by electrolyte to varying degree [24]. The infiltration of the current collector will vastly inhibit the oxygen effective transport and thus make the intrinsically sluggish oxygen diffusion more difficult. As a result, the reachable depth of oxygen is dramatically reduced, as shown in Fig. 2. What's more, the rough fluid level goes against the uniform distribution of oxygen throughout the air electrode (Supplementary Fig. S1, inset). Both of them might be reasons of the low utilization rate of the electrochemically available active sites in the normal operating conditions, especially at the high C-rate and the deep discharge. Thus, it is urgent and necessary to effectively decrease the oxygen transmission resistance and homogenize the oxygen distribution throughout the air electrode.

Herein, a TBGL (short for the triple-phase boundary guiding layer), which is not wetted by electrolyte, is designed into the conventional porous air electrode. We demonstrate that a super P-based lithium-O_2 battery in $LiClO_4$-DMSO electrolyte enables many stable cycles at a higher current density of 3000 mAh g^{-1}_{Carbon}. To our knowledge, it is far superior to that has been reported previously.

2. Experimental

2.1. Novel air electrode design and cell assembly

A particular triple-phase boundary guiding layer (abbreviated as TBGL), which was not wetted by the electrolyte, was implanted into the design of our novel air electrode. It intends to sharply prompt the effective transport of oxygen molecule to available active sites. TBGL was fabricated via impregnating the surface pretreated carbon paper (Torray, Japan) into a PTFE-based polymer emulsion under ultrasonic condition, followed by a vitrification treatment. The novel air electrode was prepared via type-casting slurry of 20 wt% polyvinlidene fluoride (PVDF) and 80 wt% super P in *N*-methyl-2-pyrrolidone (NMP, 99.9%, Aladdin) solution on the surface of TBGL (as a collector). Typically, the carbon loading density of the novel air electrode was controlled to be 0.8 ± 0.1 mg cm^{-2}. Then, the as-prepared novel air electrode was dried at 353 K for overnight and subsequently at 393 K under vacuum for more than 12 h.

The coin cell (CR 2032) and the self-designed Swagelok type battery were assembled in an argon-filled glove box (Mbraum, Germany, the contents of oxygen and moisture below 0.1 and 1 ppm, respectively) by stacking a metallic lithium foil anode (a diameter of 15 mm, 0.5 mm thickness), a glass fiber separator (Whatman GF/D) saturated by electrolyte and the as-prepared novel air electrode. 0.1 *M* electrolyte was formulated in the argon-filled glove box using dimethyl sulfoxide (DMSO, 99.7%, Aladdin) as solvent and the highest-purity lithium perchlorate ($LiClO_4$, 99.99%, metal basis, Aladdin) as solute. Prior to usage, the solvent DMSO was dehydrated over molecule sieves until the moisture content was below 6 ppm, determined by a Karl Fischer titration apparatus (Mettler-Toledo). The solute $LiClO_4$ was directly used as received. Seven holes with a diameter of 1.0 mm were evenly distributed on the CR 2032 cell positive cover so as to have easier access to outside oxygen.

2.2. XRD, SEM characterizations

The chemical compositions for the air electrode in a discharge–charge round-trip were characterized by a Rigaku D/max 2500 diffractometer (Japan, Cu Kα radiation, $\lambda = 1.54056$ Å). Scotch® tape sealed XRD holder (cubic shape, made of anodized aluminum) was utilized to hold samples for XRD analysis. The relevant XRD diffraction patterns were collected over 2θ angle range of 30°–70° at 40 kV, 200 mA. The morphology evolution on the surface of the

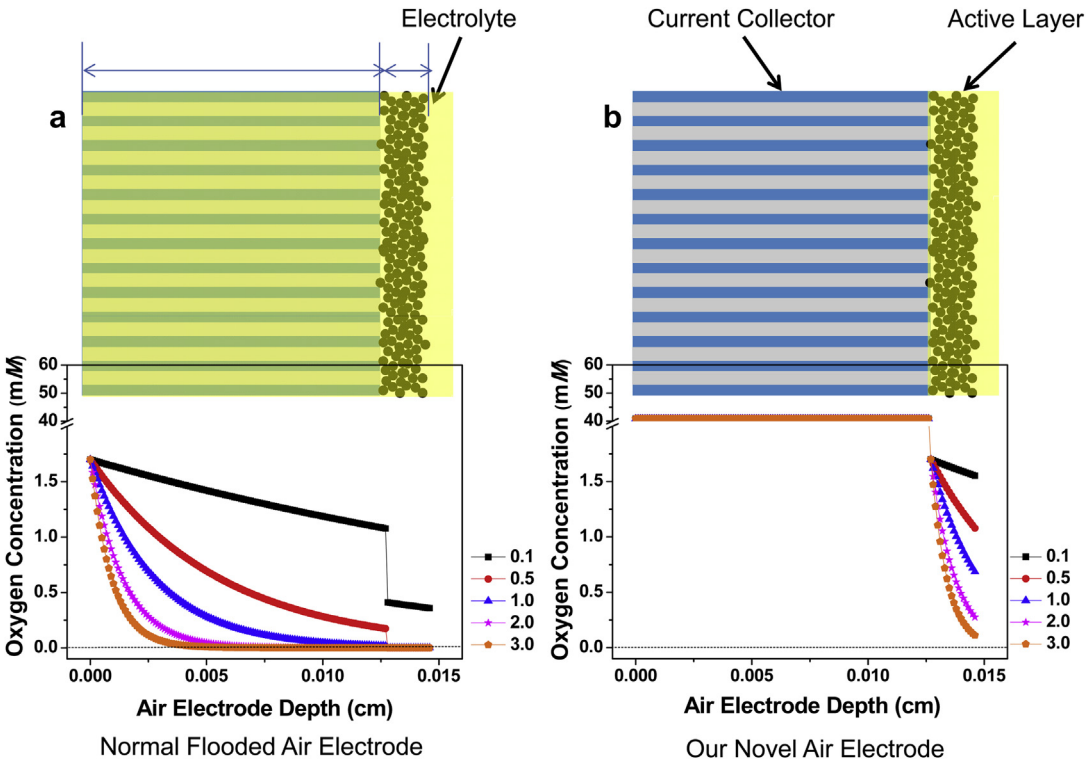

Fig. 2. Oxygen concentration distributions as a function of the current densities under the steady-state condition along the thickness of the porous air electrodes. **a** Normal flooded air electrode. **b** Our novel air electrode. Note: The current collector was simplified as a porous matrix with uniform straight channels.

air electrode during cell operation was observed by a field emission electron microscopy (FESEM, HITACH S4800, Japan) operating at 10 kV. The self-designed Swagelok type battery was specifically utilized to perform the corresponding characterizations of the phase and morphology concerned. The cycled cells were firstly disassembled in the argon-filled glove box. Then, the electrode was rinsed twice with dimethyl carbonate (DMC, anhydrous, >99%, Aldrich) and further dried for 24 h on filter paper under vacuum in order to remove the residual solvent. The sample was protected from exposure to air during the course of transfer to SEM chamber.

2.3. Electrochemical characterizations

The slow scan rate cyclic voltammetry (SSCV) experiments were carried out with a multi-channel VMP3 Biologic Instrument (France) at various scan rates in the potential range of 2.0–4.5 V (vs. Li/Li^+) to investigate the kinetics of the oxygen reduction reactions (ORRs) and the oxygen evolution reactions (OERs) occurred in the $Li/LiClO_4$-DMSO/O_2 system. The galvanostatic discharge/charge performance and the cycling stability under various current densities were evaluated via a voltage-controlled or time-controlled mode at room temperature using a Land 2001A battery testing system (Wuhan, China), respectively. For corresponding electrochemical tests, the coin cells were placed in a customized chamber filled with pure oxygen at a pressure of 1 atm. The self-designed Swagelok type cell was firstly purged by pure oxygen for approximate 30 min and then sealed except for the inlet, which was connected to a flask of oxygen at 1 atm. In both of these cases, pure oxygen passed through a molecular sieve moisture trap to prevent from the contaminations (especially moisture) before use.

3. Results and discussion

3.1. Characteristics of the novel air electrode

In our novel air electrode configuration, a key functional component, TBGL, was embedded. The specific schematic diagram was illustrated in Fig. 1. TBGL exhibited excellent unwettability against the $LiClO_4$-DMSO electrolyte as shown in Fig. 3. It was revealed that when the electrolyte was dripped on the surface of TBGL, a spherical liquid droplet was formed with a higher contact angle (θ) of more than 90°. Meanwhile the shape of the drop was basically unchanged over a long time (more than 48 h in a closed box for preventing volatility of electrolyte). In contrast, the droplet was immediately adsorbed once the electrolyte was dripped on the surface of carbon paper. Besides that, it was also discovered that when the coin cell or self-designed Swagelok type cell was taken apart after multiple cycles, the oxygen side of the novel air electrode was not wetted as expected. On account of the unwettability for the electrolyte, the implanted TBGL could contribute to better locking the electrolyte within the air electrode material zone. On the other hand, the presence of the glassy film on the surface could be favorable to establish a relatively flat gas–liquid interface (Fig. 1 & Supplementary Fig. S1). It suggests that the fundamental features of TBGL might sharply facilitate the efficient diffusion of oxygen and homogenize the oxygen distribution along the thickness of the air electrode. To certain extend, the volatility of the solvent could be effectively alleviated. Therefore, we have reason to expect that the Li-O_2 battery with our novel air electrode could exhibit the improved rate capability and the extended longer life span.

3.2. Theoretical simulation and analysis

In order to qualitatively assess the validity of TBGL on bettering the oxygen kinetics and thus greatly enhancing the high-rate performance of the lithium-oxygen battery, a diffusion-limited model for oxygen transport and conversion in the porous air electrode was established. In order to simplify the model and discussion, it was assumed that the concentration of lithium-ion in the electrolyte was sufficient enough so that the reduction reaction of oxygen could be considered as a pseudo first order process [34]. In the meantime, the shrinkage of pores during the discharge process was not considered. Theoretical calculation showed that the system could reach the stead-state condition within less than 1 min under the current density of more than 100 mA g_{Carbon}^{-1}. Thus, in steady state, the concentration of oxygen along the thickness of the porous air electrode could be represented as,

$$C_{O_2}(x) = C_{O_2}(0)\exp\left(-\frac{jx}{nFC_{O_2}(0)D_{O_2,eff}}\right) \quad (1)$$

$$D_{O_2,eff} = \frac{\varepsilon}{\tau}D_{O_2} \quad (2)$$

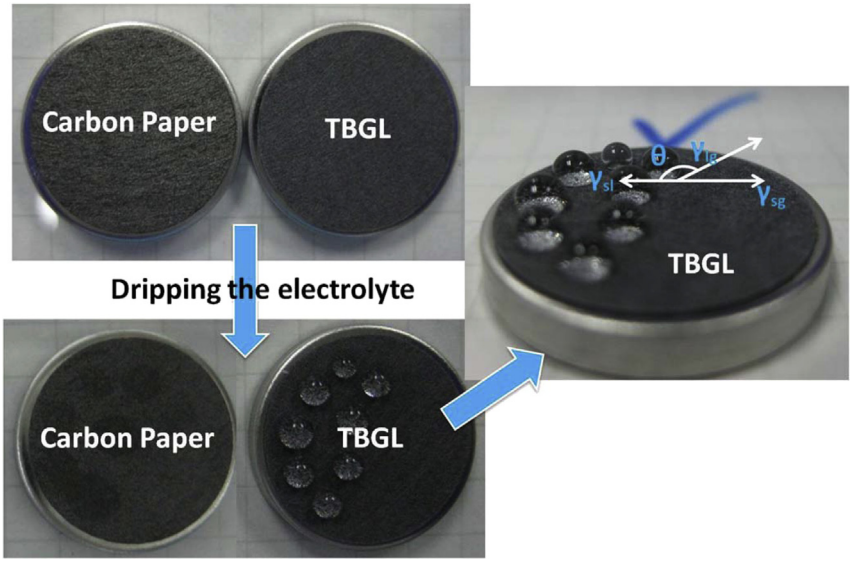

Fig. 3. Unwettability of TBGL for electrolyte.

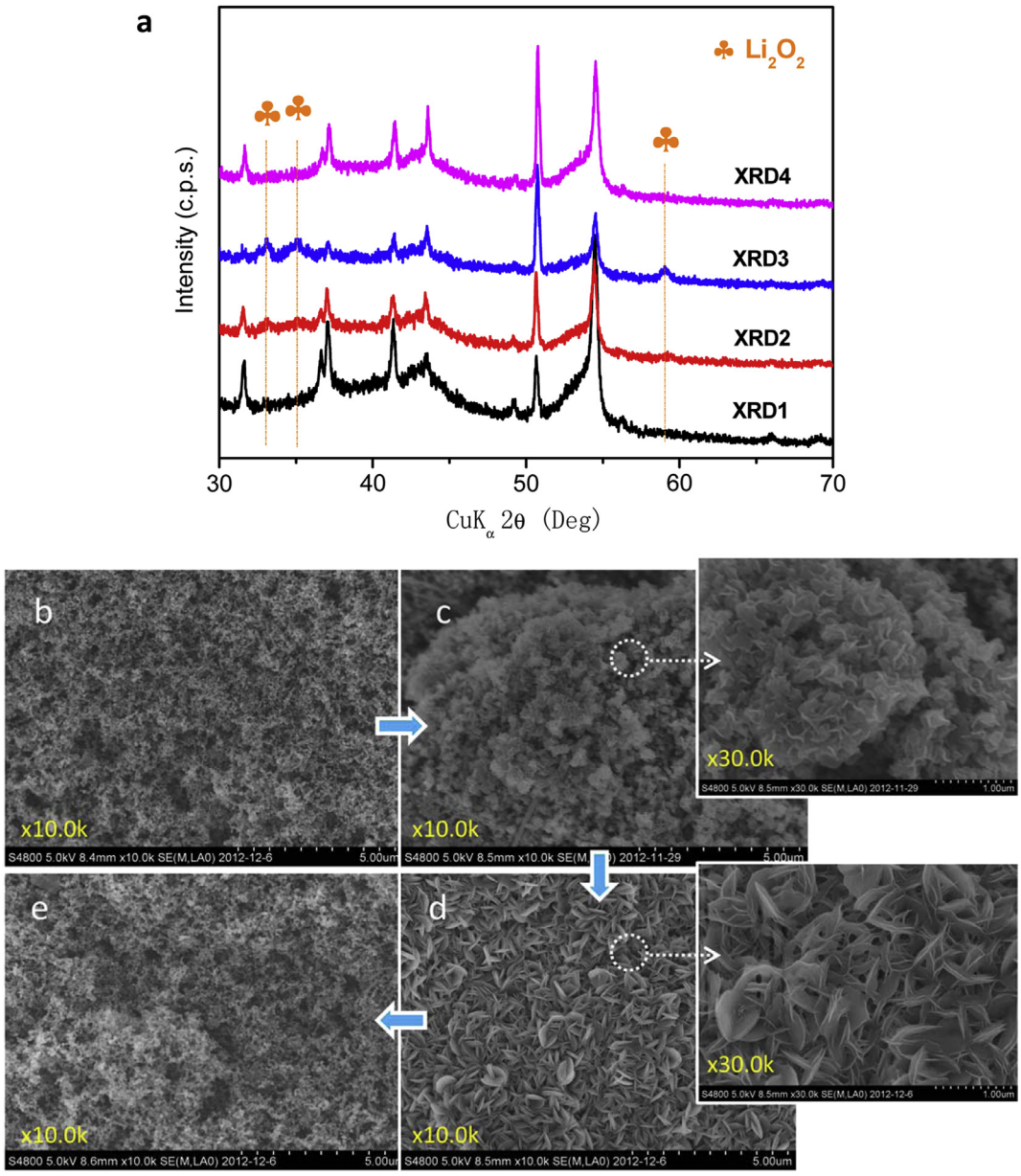

Fig. 4. Analysis for the reversible formation and decomposition of the discharge product during the discharge-recharge round-trip. **a** Results for *ex-situ* XRD analysis carried out at the original state (XRD1), 50% depth of discharge (DOD, XRD2), 100% DOD (XRD3) and at end of recharge (XRD4). **b**–**e** FESEM images of the novel air electrode. **b** before the discharge **c** at 50% DOD **d** at 100% DOD and **e** at the end of recharge.

Where, $C_{O_2}(0)$ is the initial concentration of oxygen, D_{O_2} is the oxygen diffusion coefficient in the electrolyte, $D_{O_2,eff}$ is the effective diffusion coefficient, ε is the porosity, τ is the tortuosity, j is the current density implemented, F is the Faraday constant, x is the distance which oxygen diffuses into the air electrode.

Fig. 2 shows the oxygen concentration distribution as a function of the current densities under the steady-state condition. Clearly, the diffusion depth of oxygen is heavily dependent on the discharge rates. For the conventional air electrode, because of the damping effect of the flooded current collector, the transport of oxygen to the available solid–liquid interfaces becomes extremely difficult. It was found that the oxygen concentration was weakened to be almost zero before reaching the electrode material layer under a discharge current of more than 500 mA g^{-1}_{Carbon}. In contrast, when TBGL was employed, the oxygen distribution has been dramatically improved. Even under the current density of 3000 mA g^{-1}_{Carbon}, the oxygen concentration within the super P layer is still able to afford the reduction of oxygen. Therefore, the introduction of TBGL could sharply prompt the mass-transfer of oxygen and thus provide the necessary prerequisite for the high C-rate discharge and charge.

3.3. Choice of $LiClO_4$-DMSO electrolyte

Due to strong oxidative activities, the active intermediates of Li-O_2 electrochemistry are more likely to decompose lithium salts and solvent, which would undermine the relevant electrochemical performances. Therefore, the stability of electrolyte has to be carefully considered prior to choose Li salt and solvent. The available results have indicated that $LiClO_4$ appears to be the least reactive Li salt. In $LiClO_4$-based solvent (0.8 M), less than 8% of Cl was detected in the products, which is far less than 17% of F for containing F Li salts ($LiPF_6$, $LiBF_6$ and LITFSI) [35,36]. It means that

the resultant side effect on the electrochemical performances could be very limited when $LiClO_4$-based electrolyte (0.1 M) was used. DMSO was selected as solvent mainly due to remarkable ability towards reactive reduced oxygen species. The previously results showed that the slow degradation of DMSO to $DMSO_2$ could be detected in the presence of superior anion free radical (KO_2) during 2 month period. However, no appreciable decomposition was detected when Li_2O_2 was involved in Ref. [37]. In addition, it was discovered that DMSO would be anodically oxidized above 4.2 V in the presence of trace water on Au disc electrode (3.5 V for Pt). On the basis of the short testing time (about 13 days), the low water content (6 ppm) and super P-based air electrode, it suggests that the use of DMSO may not have much of an adverse impact on the electrochemical properties of the system. Therefore in our case, we could better demonstrate the effectiveness of our novel air electrode on enhancing the rate capability and prolonging the life span.

3.4. Reversibility of the electrochemical process

The reversible formation and decomposition of Li_2O_2 was considered as a strategic point to realize the operation of the rechargeable Li-O_2 battery [2,38]. Thus, the chemical compositions of our novel air electrode during the discharge/recharge process were firstly investigated using *ex-situ* XRD analysis. As shown in Fig. 4a, the new emerging XRD diffraction peaks matched very well with the standard fingerprint of Li_2O_2 in the discharge process. After recharge, all XRD characteristic peaks corresponding to Li_2O_2 vanished again. And no odd phase (for example, LiOH, Li_2CO_3) could be detected during the discharge–charge loop. The crystallographic evidence manifests the overall reversible formation and decomposition of the dominated Li_2O_2 in the Li/$LiClO_4$-DMSO/O_2 battery without the obvious side reactions.

The reversibility of the relevant heterogeneous reaction process for our novel air electrode could be further demonstrated by *ex-situ* FESEM images, as shown in Fig. 4b–e. Before discharge, the initial electrode exhibited that nanometer super P particles (about 40 nm) were interconnected to construct a three-dimensional porous structure. When the Swagelok type cell was discharged at 500 mA g^{-1}_{Carbon} from the open-circuit voltage (OCV) to 25% depth of discharge (DOD, corresponding to a discharge specific capacity of 1000 mAh g^{-1}_{Carbon}), substance with "white fungus" shape was noticed (Fig. 4c). At the higher capacity of 4000 mAh g^{-1}_{Carbon} (100% DOD), the "petal" shaped products were found to be homogeneously covered on the surface (Fig. 4d). From FESEM images, it could be deduced that the reduction product was first evenly deposited on the surface and then gradually grew into the "petal" shaped substance via the electrochemical deposition and solid-phase diffusion processes. It is worth noting that these two kinds of morphologies are very different from "toroid" shape reported previously [14,18,20], however the same instability under the irradiation of electron beam illustrates the consistency of chemical composition of the product [18]. At the end of recharge, the porous framework of the air electrode reverted back, matching well with the particle size and shape of the initial state. The FESEM micromorphology images provide clear visual evidence to further corroborate the excellent reversibility of the Li/$LiClO_4$-DMSO/O_2 battery system.

Furthermore, it is remarkable that the whole surface of the novel air electrode is completely covered with the "petal" shaped particles after full discharge. In contrast, when the conventional air electrode (carbon paper directly as a current collector) was fully discharged up (around 2000 mAh g^{-1}_{Carbon}), the isolated "rose" shaped discharge products were randomly distributed on the surface and no "white fungus" substance was observed around them (Supplementary Fig. S2). It is quite clear that after adopting TBGL, oxygen kinetics is greatly enhanced and correspondingly, the utilization ratio of the electrochemical available solid–liquid interfaces is effectively increased. The difference in the surface morphologies between them are in accordance with the expected theoretical outcome.

3.5. Kinetics of Li-O_2 electrochemical reactions

The possible kinetic mechanisms of ORRs and OERs for our novel air electrode could be systematically investigated in the $LiClO_4$-DMSO electrolyte using a slow scan rate cyclic voltammetry (SSCV). Fig. 5a illustrates CV curves upon cycles in the voltage range of 2.0–4.5 V at a scan rate of 0.1 mV s^{-1}. The first voltammogram exhibited one reduction peak and a broad oxidation peak. In the subsequent cycles, the current was obviously suppressed in peak magnitude. The significant decrease of peak intensity could be explained by the reduction of the electronic conductivity of air electrode, which might attribute to the incomplete decomposition of the reduction specie Li_2O_2 in the previous cycle. On the surface of it, the result seems to contradict the above conclusion (XRD and SEM) of the reversible formation and decomposition of the dominated Li_2O_2. In fact, it was mostly caused by the difference in the characterization

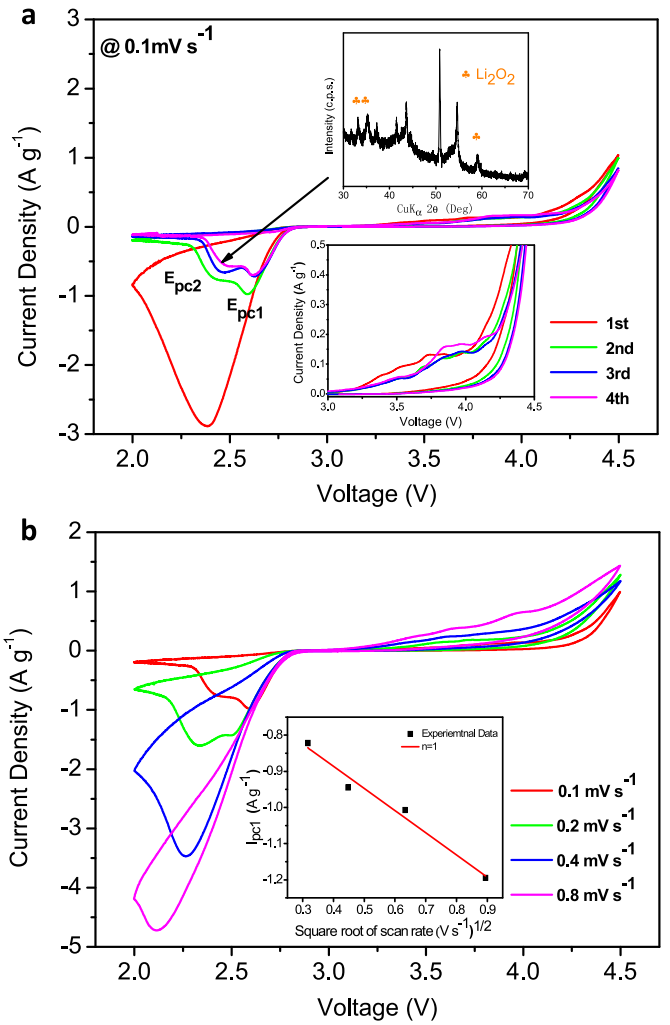

Fig. 5. CV curves of the novel air electrode in Li/$LiClO_4$-DMSO/O_2 battery. **a** CV profiles upon cycling at a scan rate of 0.1 mV s^{-1}. Inset: Topside for *ex-situ* XRD profile of the air electrode discharged at 2.4 V; Underside for CV curves in the potential range of 3.0–4.5 V. **b** CV profiles under various scan rates. Inset: Graph of the normalized peak current at E_{pc1} vs. the square root of the scan rate.

approaches of the SSCV and the galvanostatic discharge/charge test. Additionally, more than one cathodic peak could be found, signifying the existence of the two electrochemical events. Therefore, it is meaningful to decode the complexity of the electrochemical events involved and further identify the specific electrochemical event occurred at each cathodic peak position.

In the Li^+-conducting aprotic electrolyte, the reduction of O_2 molecules proceeds in order of the formation of the products, from $O_2^{\cdot-}$ (LiO_2) to O_2^{2-} (Li_2O_2) and to O^{2-}(Li_2O) [17]. And owing to the higher stability of intermediate $O_2^{\cdot-}$ in DMSO, upon scanning cathodically further, the undecomposed or survived LiO_2 could further reacts with Li^+ and e^- to generate Li_2O_2 (Supplementary Fig. S3) [17,39]. Therefore, it is very likely that the cathodic peak (E_{pc2}) at the lower potential (Fig. 5a) could be ascribed to the further reduction of LiO_2 to Li_2O_2. In order to figure out which electrochemical reaction happened at about 2.4 V, the *ex-situ* XRD analysis was employed. The XRD profile showed that the chemical composition of the ORRs product was identified as Li_2O_2 instead of Li_2O (in Fig. 5a, inset). Thus, it is safe to conclude that the first cathodic peak (E_{pc1}) at around 2.6 V and the second one (E_{pc2}) at about 2.4 V could be associated with the oxygen/superoxide redox couple and the further reduction of LiO_2, respectively. It was the first time that these two redox electrochemical processes were successfully separated and detected in the aprotic solvent. In sum, the mechanism of ORRs in the Li/$LiClO_4$-DMSO/O_2 system could be represented by the reactions involving the formation of the $Li^+ - (DMSO)_4 - O_2^-$, which is decomposed and partly reduced further to form Li_2O_2 [17,39]. It was unequivocally stated that at the end of the discharge, the final discharge product was dominated by Li_2O_2, in good line with the XRD results.

Consequently, the appearance of the single peak in the first cycle might be explained by assuming an electrochemical activation process related to the sluggish diffusion of oxygen [9]. In this step, lithium-ion reacts with the insufficient superoxide $O_2^{\cdot-}$ generated, which might result from an initial, uneven distribution or inadequate diffusion of oxygen throughout the bulk of the air electrode [39]. In fact, this behavior could be observed in our galvanostatic discharge and charge curves mentioned below. Besides, compared with the normal air electrode, the novel air electrode exhibited larger peak current (Supplementary Fig. S4), indicating the enhanced oxygen diffusion. The results fully proved the effectiveness of TBGL on improving the oxygen diffusion.

Reversing the sweep at 2.0 V, multiple anodic peaks were observed in the voltage range of 3.0–4.3 V (Fig. 5a, inset). Combined with the XRD analysis, the result indicated that these anodic peaks could be ascribed to the consecutive decompositions of Li_2O_2 in various pores or on diverse surface orientations [40]. The similar CV response has been described in porous electrodes [8,16]. Hence, the mechanism of OERs could be expressed by the oxidation of Li_2O_2, which is in good agreement with the previous results [17].

The scan rate dependence of ORRs on our novel air electrode was investigated in order to further quantify the electron transfer at about 2.6 V during the irreversible oxygen reduction in the Li/$LiClO_4$-DMSO/O_2 battery. The plot of the normalized peak current density with the square root of the scan rate shows a linear dependence (Fig. 5b, inset), indicating that the irreversible process is a diffusion-controlled electrochemical reaction. Hence, a Nicholson–Shain equation (3) could be applied in the further analysis of CV [41].

$$i_p = 2.99 \times 10^5 n\left(\alpha^{\frac{1}{2}} n^{*\frac{1}{2}}\right) A D^{\frac{1}{2}} C v^{\frac{1}{2}} \quad (3)$$

Where, i_p is the cathodic peak current (A), α is the transfer constant, A is the projected area of the air electrode (cm^2), n is the electron number participating in redox reaction per mol, n^* is the number of electrons involved in the diffusion-controlled process, D is the diffusion coefficient of oxygen, C is the concentration of O_2 (M) in the electrolyte, v is the scan rate ($V\ s^{-1}$). The concentration of oxygen in DMSO was calculated to be approximately 0.0017 M by Henry's law from Bunsen coefficient α of DMSO ($a = 0.0416$). D could be calculated by a Stokes–Einstein equation as followed,

$$D = \frac{k_B T}{6\pi\eta R_H} \quad (4)$$

where, k_B is the Boltzmann constant (1.38×10^{-23} J K^{-1}), η is the viscosity of DMSO (1.996 cps), R_H is the hydrodynamic radius of O_2 (121 pm). According to Equation (4), the diffusion coefficient of oxygen was calculated to be 9.04×10^{-6} $cm^2\ s^{-1}$.

Therefore, Equation (3) could be translated into Equation (5)

$$i_{p=} 1.53n\left(\alpha^{\frac{1}{2}} n^{*\frac{1}{2}}\right) v^{\frac{1}{2}} \quad (5)$$

As observed in inset of Fig. 5b, if both n and n^* are set to equal to 1 theoretically, the experimental data can be fitted well by the theoretical slope when $\alpha = 0.16$. Given the irreversible electrochemical reduction reaction, the value of α is reasonable. According to the fitting results, it could make a conclusion that a one-electron transfer reaction occurred at the first reduction peak (E_{pc1}) and LiO_2 was more likely the predominated discharge product.

3.6. Rate capability

Generally, the specific capacity of Li-O_2 cells was reported in terms of mAh g^{-1}_{Carbon}. In our novel air electrode, carbon paper and the polymer emulsion were involved. Thus, it is necessary to remove the contribution from TBGL in the matter of the specific capacity. As shown in Fig. 6 inset, when only TBGL was acted as the air electrode, a capacity of no more than 70 mAh g^{-1} was delivered under the current magnitude of 0.088 mA. The result is similar to that reported by Jung et al. [9]. Apparently, the capacity of TBGL alone in the uptake of lithium-ion is quite limited. Therefore, it is reasonable to neglect the performance impact of TBGL.

The rate capability of our novel super P-based air electrode in the Li/$LiClO_4$-DMSO/O_2 battery was performed under various current rates, as shown in Fig. 6. At a current density of 200 mA g^{-1}_{Carbon} (equivalent to 0.16 mA cm^{-2}), the novel air electrode exhibited a flat

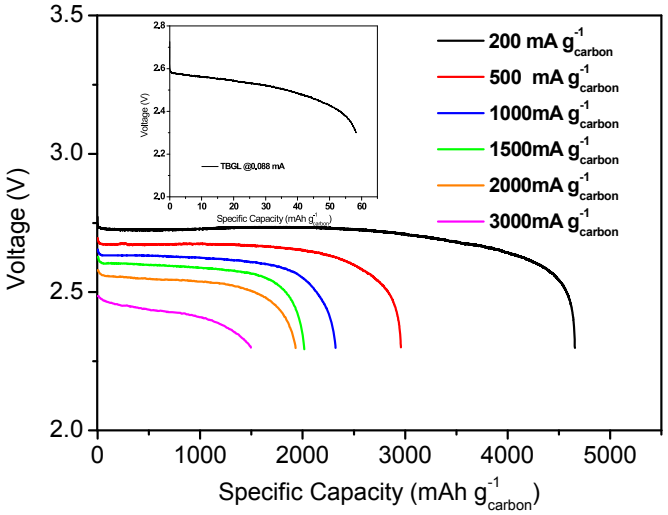

Fig. 6. Discharge curves of the Li–O_2 battery using the novel air electrode at various current densities. Inset: Discharge curves of a blank Li–O_2 cell only using TBGL as air electrode.

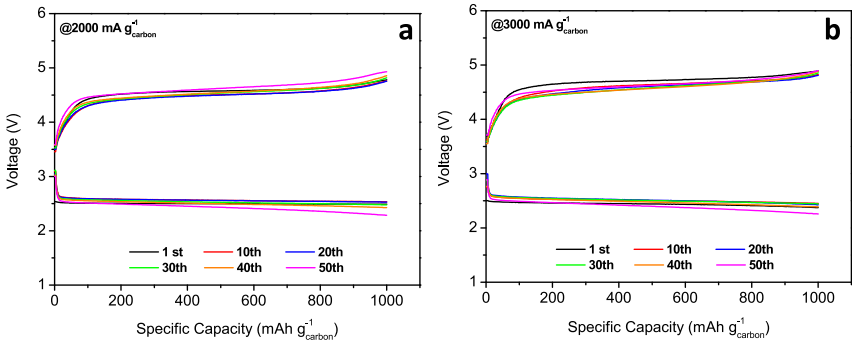

Fig. 7. Cycling stability of the novel air electrode at a discharge capacity limit of 1000 mAh g^{-1}_{Carbon} at different current densities. **a** at 2000 mA g^{-1}_{Carbon}. **b** at 3000.mAh g^{-1}_{Carbon}.

discharge plateau of approximately 2.7 V and a high discharge capacity of around 4700 mAh g^{-1}_{Carbon}. The discharge capacity delivered is comparable with that exhibited by other carbon-based materials with higher mesopore volume or novel hierarchically porous, such as KB carbon [20,21] and graphene oxide-derived carbon [20]. In some cases, the performance is even more superior to or matched to that displayed by carbon-based materials (e.g. super P [42], Au catalyzed Vulcan carbon [10], hollow carbon fiber [18]) as DME-based (dimethoxyethane) electrolyte with higher kinetic parameters was employed (Supplementary Fig. S5). The results indicated that the introduction of TBGL brought about a striking effect on the enormous increase of the utilization ratio of the potential electrochemical active sites.

With the increase of the current density, the superior of our novel air electrode in the energy storage becomes more apparent. It has far outweighed the best attainable level achieved by carbonaceous materials in DMSO-based electrolyte [20,21]. When the current density was approximately as high as 3000 mA g^{-1}_{Carbon} (equivalent to 2.4 mA cm^{-2}), a higher specific capacity of 1500 mAh g^{-1}_{Carbon} was still achieved. For the conventional carbon-based air electrode, such a high current density is very difficult to be afforded. So far, only limited papers involving in DME (P_{O2} ~ 2 atm), TEGDME (tetra(ethylene) glycol dimethyl ether; P_{O2} ~ 1 atm) and 1-ethyl-3 methylimidazolium bis(trifluoromethylsulfonyl) covered the operation of the lithium-oxygen battery under such a large current density [9,43,44]. Obviously, in view of the lower oxygen solubility and diffusion coefficient of DMSO, the enhancement of the rate capability mainly owes to the effectiveness of TBGL on improving the oxygen kinetics.

In addition, it is interesting that our air electrode design is not unique but universal. When the spherical polypyrrole particles were used as electrode materials, the lithium-oxygen battery also exhibited better rate performance, as shown in Supplementary Fig. S6. At the current of 200 mA g^{-1}, the specific capacity of about 4300 mAh g^{-1} was delivered. When the current density was increased to about 1000 mA g^{-1}, around 50% capacity was still retained. It is much better than that exhibited by granular or nanotubular polyprrole in the 0.1 *M* LiTFSI (lithium trifluoromethane sulfonimide)-DME electrolyte [24]. At the same time, when NMP (*N*-methyl-2-pyrrolidone) as a solvent, the similar performance improvements were expressed (Supplementary Fig. S7).

3.7. Cycling performance

Note that close to 70% of the discharge specific capacity (1000 mAh g^{-1}_{Carbon}) delivered at C-rate of 3000 mA g^{-1}_{Carbon} was used as a benchmark to characterize the cycle stability of the Li/$LiClO_4$-DMSO/O_2 system at various C-rates. Fig. 7a, b represented the discharge-charge curves for the novel air electrode at fairly high current rates of 2000 and 3000 mA g^{-1}_{Carbon}, respectively. Followed by an electrochemical activation process discussed in commenting on Fig. 5a, the profiles overlap and the coin cells exhibit stable electrochemical behaviors, demonstrating over 50 stable cycles. On the contrary, the conventional flooded air electrode just could be steadily cycled at 1000 mA g^{-1}_{Carbon} (Supplementary Fig. S8). The experimental results are in accordance with the calculation results. Till now, majority of the research work on Li-O_2 battery only limited the current densities to no more than 1000 mA g^{-1}_{Carbon} on the basis of rechargeability. In our case, due to the advantageous kinetics, the maximum on-load current density was tripled. It meant the discharging/charging time was reduced to 20 min for a capacity of 1000 mAh g^{-1}_{Carbon}. Based on the weight of the super P and the resultant Li_2O_2, the specific power density could reach 4040 W kg^{-1}; even so, a substantial specific energy of 1350 Wh kg^{-1} could still be achieved. The energy density is close to the usable specific energy of gasoline for automotive application (c.a. 1700 Wh kg^{-1}) [45]. The power density is four times than the general requirements proposed by the electric vehicles (1000–1500 W kg^{-1}) [43]. Clearly, the improvement of the electrochemical performance has an inner close connection with the enhanced dynamics of oxygen throughout the air electrode. This finding proposes a new feasibility to accomplish the heavy load discharge performance by means of the novel air electrode design.

As for the Li–O_2 battery with a unique open architecture, the volatility of solvent has been always an inevitable question to address. In order to allow a positive evaluation on the role of TBGL in alleviating the volatility of solvent, all the coin cells were placed into the custom made chamber (about 140 L). It was found that the introduction of TBGL effectively suppresses the volatile problem and thus significantly extends the life span. At the low current density of 500 mA g^{-1}_{Carbon}, the conventional air electrode could only be cycled about 20 times (approximately 93 h) as a result of much more loss of the solvent (Supplementary Fig. S8). Conversely, when the novel air electrode was put into use, it exhibited no less than 29 stable cycles (over 127 h) as shown in Fig. 8a. & Supplementary Fig. S8. The operating time was extended by approximately 37%. Even if compared with the event the cell was sealed in 3 mil bag (100 h @ 100 mA g^{-1}_{Carbon}) [21], the effect on extending the runtime is more pronounced. It is quite clear that the greater longevity is ascribed to the introduction of TBGL. In fact, the volatility of solvent could be further alleviated by using our self-designed Swagelok type battery. It was demonstrated that the novel air electrode could be steadily cycled over 70 times (more than 300 h) at a current of 500 mA g^{-1}_{Carbon} and a limiting capacity of 1000 mA g^{-1}_{Carbon}, as showed in Fig. 8b. It is easy for us to notice that it is already a major advance for the nonaqueous Li-O_2 cell, especially for the DMSO system.

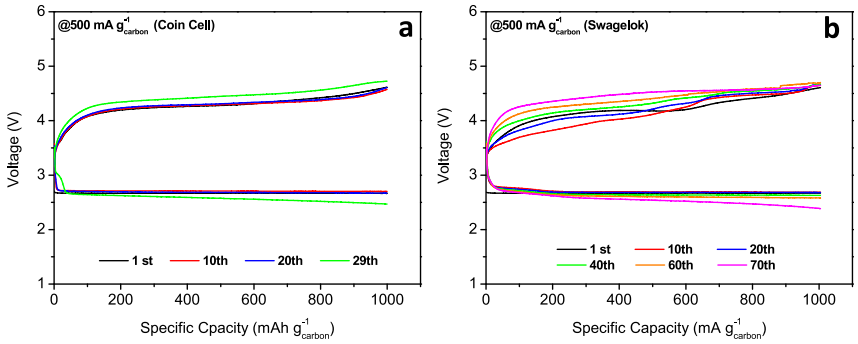

Fig. 8. Cycling stability of the novel electrode in $LiClO_4$-DMSO electrolyte for different battery types at a current density of 500 mA g^{-1}_{Carbon} and a specific capacity limit of 1000 mAh g^{-1}_{Carbon}. **a** CR 2032 coin cell. **b** Self-designed Swagelok type cell.

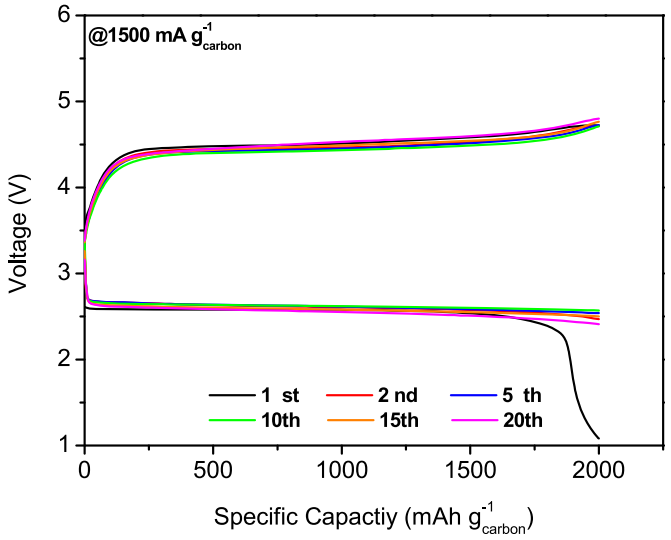

Fig. 9. Current-voltage curves of the Li–O_2 battery using the novel air electrode at a current density of 1500 mA g^{-1}_{Carbon}.

Finally, we extended the related electrochemical performance characterizations by exploiting the cyclic response under the maximum discharge specific capacity. The influence of the capacity limit at 1500 mA g^{-1}_{Carbon} (corresponding to a specific capacity of about 2020 mAh g^{-1}_{Carbon}, as shown in Fig. 6) on the cyclic stability was investigated. Fig. 9 presents the discharge-charge profiles, demonstrating that the cell could be run over 20 stable cycles at near full discharge-charge. It once again corroborated the excellent cycling stability of our designed Li-O_2 battery at the higher capacity.

4. Conclusion remark

In summary, we have successfully designed a novel air electrode with excellent unwettabilty for the electrolyte to address the poor rate capability and short calendar life. It is demonstrated that our super P-based novel air electrode can be steadily cycled over 50 times at a current density as high as 3000 mA g^{-1}_{Carbon} and a discharge depth of 1000 mAh g^{-1}_{Carbon}, which corresponds a discharge/charge time of about 20 min. The high current density and power density (about 4040 W kg^{-1}) achieved are a best record for the Li-O_2 battery reported to date. This remarked electrochemical performance is attributed to the implantation of the critical component TBGL. The introduction of TBGL is beneficial to facilitate the diffusion of oxygen throughout the whole air electrode, increase the utilization ratio of the electrochemically available active sites, and slow down the volatility of the electrolyte to some extent. By focusing on design of the air electrode based on the nature of electrolyte, we dedicated to opening up a brand new view to greatly boost the electrochemical performances for lithium-O_2 battery, especially the high C-rate property.

Acknowledgments

We thank the financial support from China National Science Foundation-Youth Scientific Foundation (No. 51302147), China Postdoctoral Science Foundation (No. 2012M510022) and Shenzhen Special funds for the Emerging Strategic Industry Development (NO. JCYJ20120616220714779). We also appreciate the financial support from Guangdong Province Innovative R&D Team Plan.

Appendix A. Supplementary data

Supplementary data related to this article can be found at http://dx.doi.org/10.1016/j.jpowsour.2013.12.124.

References

[1] P.G. Bruce, S.A. Freunberger, L.J. Hardwick, J.-M. Tarascon, Nat. Mater. 11 (2012) 19–29.
[2] Y. Shao, F. Ding, J. Xiao, J. Zhang, W. Xu, S. Park, J.-G. Zhang, Y. Wang, J. Liu, Adv. Funct. Mater. (2012), http://dx.doi.org/10.1002/adfm.201200688.
[3] J. Christensen, P. Albertus, R.S. Sanchez-Carrera, T. Lohmann, B. Kozinsky, R. Liedtke, J. Ahmed, A. Kojic, J. Electrochem. Soc. 159 (2012) R1–R30.
[4] B. Scrosati, J. Hassoun, Y.-K. Sun, Energy Environ. Sci. 4 (2011) 3287–3295.
[5] K.M. Abraham, Z. Jiang, J. Electrochem. Soc. 143 (1996) 1–5.
[6] V.S. Bryantsev, V. Giordani, W. Walker, M. Blanco, S. Zecevic, K. Sasaki, J. Uddin, D. Addison, G.V. Chase, J. Phys. Chem. A. 115 (2011) 12399–12409.
[7] V.S. Bryabtsev, F. Faglioni, J. Phys. Chem. A. 116 (2012) 7128–7138.
[8] Z. Peng, S.A. Freunberger, Y. Chen, P.G. Bruce, Science. 337 (2012) 563–566.
[9] H.-G. Jung, J. Hassoun, J.-B. Park, Y.-K. Sun, B. Scrosati, Nat. Chem. 4 (2012) 579–585.
[10] Y.-C. Lu, D.G. Kwabi, K.P.C. Yao, J.R. Harding, J. Zhou, L. Zuin, Y. Shao-Horn, Energy Environ. Sci. 4 (2011) 2999–3007.
[11] S.A. Freunberger, Y. Chen, N.E. Drewett, L.J. Hardwick, F. Barde, P.G. Bruce, Angew. Chem. Int. Ed. 50 (2011) 8609–8613.
[12] S.A. Freunberger, Y. Chen, Z. Peng, J.M. Griffin, L.J. Hardwich, F. Barde, P. Novak, P.G. Bruce, J. Am. Chem. Soc. 133 (2011) 8040–8047.
[13] Y. Chen, S.A. Freunberger, Z. Peng, F. Bardé, P.G. Bruce, J. Am. Chem. Soc. 134 (2012) 7952–7957.
[14] D. Capsoni, M. Bini, S. Ferrari, E. Quartarone, P. Mustarelli, J. Power. Sources 220 (2012) 253–263.
[15] J. Read, K. Mutolo, M. Ervin, W. Behl, J. Wolfenstine, A. Driedger, D. Foster, J. Electrochem. Soc. 150 (2003) A1351–A1356.
[16] B.D. McCloskey, D.S. Bethune, R.M. Shelby, G. Girishkumar, A.C. Luntz, J. Phys. Chem. Lett. 2 (2011) 1161–1166.
[17] C.O. Laoire, S. Mukerjee, K.M. Abraham, J. Phys. Chem. C. 114 (2010) 9178–9186.
[18] R.R. Mitchell, B.M. Gallant, C.V. Thompson, Y. Shao-Horn, Energy Environ. Sci. 4 (2011) 2592–2598.
[19] S.R. Younesi, S. Urbonaite, F. Björefors, K. Edström, J. Power Sources 196 (2011) 9835–9838.
[20] D. Xu, Z. Wang, J. Xu, L. Zhang, X. Zhang, Chem. Commun. 48 (2012) 6948–6950.

[21] M.J. Trahan, S. Mukerjee, E.J. Plichta, M.A. Hendrickson, K.M. Abraham, J. Electrochem. Soc. 160 (2013) A259–A267.
[22] Y. Li, J. Wang, X. Li, D. Geng, R. Li, X. Sun, Chem. Commun. 47 (2011) 9438–9940.
[23] H. Wang, Y. Yang, Y. Liang, G. Zheng, Y. Li, Y. Cui, H. Dai, Energy Environ. Sci. 5 (2012) 7391–7935.
[24] Y.-C. Lu, Z. Xu, H.A. Gasteiger, S. Chen, K. Hamad-Schifferli, Y. Shao-Horn, J. Am. Chem. Soc. 132 (2010) 12170–12171.
[25] Y. Cui, Z. Wen, X. Liang, Y. Lu, J. Jin, M. Wu, X. Wu, Energy Environ. Sci. 5 (2012) 7893–7897.
[26] Y.-C. Lu, H.A. Gasyeiger, Y. Shao-Horn, J. Phys. Chem. Soc. 133 (2011) 19048–19051.
[27] Y. Shao, S. Park, J. Xiao, J.-G. Zhang, Y. Wang, J. Liu, ACS Catal. 2 (2012) 844–857.
[28] A. Débart, A.J. Paterson, J. Bao, P.G. Bruce, Angew. Chem. 120 (2008) 4597–4600.
[29] S.H. Oh, R. Black, E. Pomerantseva, J.-H. Lee, L.F. Nazar, Nat. Chem. 4 (2012) 1004–1010.
[30] J.R. Harding, Y.-C. Lu, Y. Tsukada, Y. Shao-Horn, Phys. Chem. Chem. Phys. 14 (2012) 10540–10546.
[31] L. Trahey, N.K. Karan, M.K.Y. Chan, J. Lu, Y. Ren, J. Greeley, M. Balasubramanian, A.K. Burrell, L.A. Curtiss, M.M. Thackeray, Adv. Energy Mater. (2012), http://dx.doi.org/10.1002/AENM.201200037.
[32] B.D. McCloskey, R. Scheffer, A. Speidel, D.S. Bethune, R.M. Shelby, A.C. Luntz, J. Am. Chem. Soc. 133 (2011) 18038–18041.
[33] J.-L. Shui, N.K. Karan, M. Balasubramanian, S.-Y. Li, D.–J. Liu, J. Am. Chem. Soc. 134 (2012) 16654–16661.
[34] S.S. Sandhu, J.P. Fellner, G.W. Brutchen, J. Power Sources 164 (2007) 365–371.
[35] G.M. Veith, J. Nanda, L.H. Delmau, N.J. Dudney, J. Phys. Chem. Lett. 3 (2012) 1242–1247.
[36] R. Younesi, M. Hahlin, K. Edstrom, ACS Appl. Mater. Interfaces 5 (2013) 1333–1341.
[37] N. Mozhzhukhina, L.P. Mendea De Leo, E.J. Calvo, J. Phys. Chem. C. 117 (2013) 18375–18380.
[38] T. Ogasawara, A. Débart, M. Holzapfel, P. Novák, P.G. Bruce, J. Am. Chem. Soc. 128 (2006) 1390–1393.
[39] Z. Peng, S.A. Freunberger, L.J. Hardwick, Y. Chen, V. Giordani, F. Barde, D.P. Novak, D. Graham, J.–M. Tarascon, P.G. Bruce, Angew. Chem. Int. Ed. 50 (2011) 6351–6355.
[40] Y. Mo, S. Ping Ong, G. Ceder, Phys. Rev. B 84 (2011) 205446.
[41] R.S. Nicholson, I. Shain, Anal. Chem. 36 (1964) 706–723.
[42] H. Wang, K. Xie, Electrochem. Acta 64 (2012) 29–34.
[43] T. Zhang, H. Zhou, Angew. Chem. Int. Ed. 51 (2012) 11062–11067.
[44] Z. Wang, D. Xu, J.-J. Xu, L.-L. Zhang, X.-B. Zhang, Adv. Funct. Mater. 22 (2012) 3699–3705.
[45] G. Girishkumar, B. McCloskey, A.C. Luntz, S. Swanson, W. Wilcke, J. Phys. Chem. Lett. 1 (2010) 2093–2203.